Flexible Thermistors based on Laser-Induced Graphene from Polyetherimide

Yann Houeix[1*], Shayma Habboush[1], Sonia Gomez-Gijon[1], Noel Rodriguez[1], Francisco J. Romero[1] and Almudena Rivadeneyra[1*]

[1] Department Electronics and Computer Technology, University of Granada, Granada, Spain.
*Authors to whom any correspondence should be addressed.

E-mail: yannhx@ugr.es, arivadeneyra@ugr.es

Abstract

The importance of temperature sensors has notably increased in recent years, paralleling the surge in demand for flexible and stretchable sensor technologies. In this study, we fabricate and characterize a flexible resistive temperature sensor based on Laser-Induced Graphene (LIG) on Polyetherimide (PEI). The structure and morphology of LIG are thoughtfully characterized proving the formation of a graphitic-based structure. Subsequently, the sensors were evaluated in terms of their temperature response, impact of relative humidity (RH), and bending cycles. The results reveal that the PEI-LIG flexible thermistor exhibits a high sensitivity of -0.159%/°C, with minimal influence from humidity. These findings contribute to advancing the research in inexpensive flexible temperature sensing technology, providing insights into material selection and sensor design for diverse applications.

Keywords: flexible electronics, thermistor, LIG, polyetherimide, sensor characterization.

1. Introduction

Temperature plays a key role in various technological applications so there is a need for its enhanced precision sensing and real-time monitoring. Diverse applications are emerging for flexible and stretchable sensors in fields like the food industry [1], machines [2] and human body [3]. Moreover, promising applications such as human-machine interfaces [4] and health monitoring [5] demand compatibility with free-form surfaces, where such features are essential for their effective implementation. Additionally, with the paradigm of the Internet of Things (IoT), where there is a continuously increasing number of devices interconnected, the need for cost-effective, mass-produced, and eco-friendly sensors is primordial. In this sense, the most widely used temperature sensors are the thermistors, a type of resistor whose resistance is strongly dependent on temperature. Common thermo-sensitive materials used in this context are ceramics [6], metal alloys [7] and polymers [8] whose resistance changes proportionally with the temperature. The advantages of the ceramic thermistor are its low cost, high sensitivity, and fast response. However, they are generally rigid making impossible its adaptation to any non-planar surface. Metal alloys are the most used with good sensitivity and stability, but they are more expensive and have a greater environmental impact. Conversely, conductive polymers are compatible with free-form surfaces but exhibit lower sensitivity and repeatability.

Despite the widespread use of these types of thermistors, none of them combines all the desired properties, i.e., good sensitivity, low cost, fast response, flexibility, and environment-friendliness simultaneously. To address all these desired features, the research in new materials, specifically in carbon-based materials is actively being investigated. In particular, graphene [9] and graphene-based materials [10], such as graphene oxide (GO) [11], reduced graphene oxide (rGO) [12] or carbon nanotubes (CNT) [13] are broadly employed for flexible temperature sensors. However, all these techniques involve energy-intensive processes and heavy chemical treatments, raising environmental concerns [14,15]. As a promising alternative, Laser-Induced Graphene (LIG) has garnered interest since its discovery in 2014 [16]. This technique involves treating a carbon-rich precursor with a laser, converting the raw insulator substrate into a conductive material via laser photothermal or photochemical effects [17]. LIG offers a single-step, mask-less, and chemical-free fabrication process, enabling complex pattern designs and conductivity tuning.

This technique has been proved from multiple substrates, from GO to diverse polymer substrates and natural materials [18,19]. However, the use of natural substrates, such as paper,

wood or cork, is usually associated with adding fire retardant treatments and results in a lower sensibility and reproducibility [20,21]. Consequently, polymer substrates, particularly Kapton© polyimide (PI), are widely employed in LIG due to their flexibility and versatility in multiple applications, ranging from chemical and physical sensors to energy storage [22,23]. The use of other polymers has also been reported, such as polyetherimide [24–26], polyetheretherketone (PEEK) [17] or polymetaphenylene isophthalamide (Nomex) [28]. Notably, PEI stands out for its exceptional properties and cost-effectiveness compared to other substrates, making it an excellent choice for LIG. In a previous work [29], the authors compare the properties of LIG on PI and PEI for electrochemical applications, concluding that LIG from PEI exhibits improved electrical conductivity with a more robust and homogenous morphology. In this context, LIG temperature sensors have already been studied on PI [30–32], GO [33,34] and on paper [20], although no research on LIG thermistors based on PEI has been reported yet. These sensors, fabricated directly on the flexible polymer surface, can be easily attached to any curved surface, eliminating the need for the transfer process required in traditional CVD graphene synthesis.

After explaining the fabrication and characterization methods, this paper presents a study of the characterization of LIG materials on PEI substrate through Raman spectroscopy, X-ray photoelectron spectroscopy (XPS) and Scanning Electron Microscope (SEM). Subsequently, two thermistor designs were fabricated. Both transducers were tested in a climate chamber to characterize the temperature response, the effect of the relative humidity (RH) and the bending behaviour. Finally, the main conclusions are drawn up.

2. Materials and methods

2.1 Materials

The polymer used in this work is ULTEM™ 1000 Polyetherimide (PEI) sheet from Prima Filaments®, with a thickness of 200 µm, and an additional 35 µm of adhesive on the back. Prior to the laser scribing process, the surface of the material is cleaned with isopropyl alcohol. Subsequently, after drying for 1 minute, the material was directly laser scribed.

2.2 Devices fabrication

The laser scribing process was performed using a PowerLine E-12-532 Laser by Coherent® (Munich, Germany) at ambient conditions as illustrated in figure 1. This setup uses a galvanometric pulsed laser with a wavelength of 532 nm (green light). The scribing process occurs at the focal point (270 mm), obtaining a laser spot of 1.6 ± 0.2 mm, and the distance between two passes is set to 70 µm.

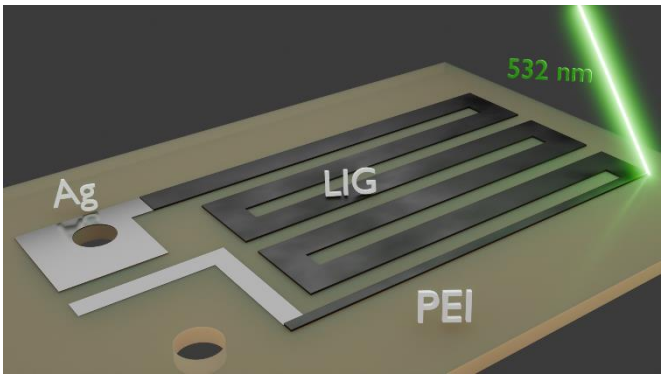

Figure 1. Schematic of the fabrication of LIG thermistor on PEI with the connexion made with silver ink.

Two serpentine thermistor designs were created, as illustrated in figure 2: a small design measuring a total length of 136.5 mm, and a large design measuring a total length of 268.0 mm, both with a width of the pattern of 1.5 mm. For the LIG on PEI substrate, two passes are required to achieve the desired high resistivity. The first pass seeks to form a non-conductive amorphous carbon black layer, while the following pass forms the high resistive layer of LIG [18]. In this case, the first pass uses a power of 2 W at a speed of 100 mm/s, and the second pass uses a power of 1.5 W at a speed of 55 mm/s. These parameters are selected to achieve a homogenous LIG layer with a resistance high enough to reduce both the self-heating effect and the power consumption. Under ambient conditions (~25°C, ~35%RH), the LIG on PEI thermistor exhibited resistances of 182.2 ± 6.7 kΩ and 83.6 ± 3.3 kΩ for the large and small designs, respectively. The frequency response of both designs is presented in figure S.1, showing pure resistive behaviour. The transducers were connected using a screw-mounted SubMiniature version A (SMA) Series End Launch Connector from Bulgin® (Santa Fe, CA, USA), with a thin layer of RS® PRO conductive silver lacquer applied near the edge of the connector to complete the contact.

2.3 Material characterization

Raman spectrometer analyses were carried out by the Micro-Raman Jasco NRS-5100 (Easton, PA, USA) system, using a green diode of 532 nm as the excitation source.

The X-ray Photoelectron Spectroscopy was carried out on a Kratos Axis Ultra-DLD (Manchester, UK), using a power and step energy of 75 W and 160 eV for general spectra, and 150 W and 40 eV for higher resolution. The spectra were analyzed with CASA software with reference to adventitious C_{1s}, at 285 eV.

Keysight® B2902A Source Meter Unit (SMU) (Santa Rosa, California, USA) was used to measure voltage and current for the electrical characterization of the LIG sheet resistivity together with the four-probe station Universal Probe Station from Jandel® (Eggington, UK) with a spacing between needles of 1.0 mm. The method used to evaluate the

sheet resistance is the In-Line Four-Point Probe with the Dual-Configuration [35]. The sheet resistance of the LIG obtained with the selected laser parameter is 870 ± 100 Ω/sq.

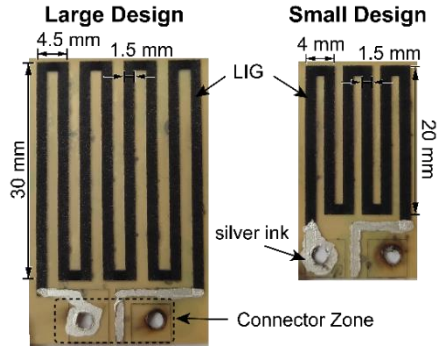

Figure 2. Photography of PEI LIG thermistors with their corresponding dimensions.

2.4 Sensor characterization

The climate chamber used to test the sensors was the LabEvent L C/34/70/5 from Weiss Technik® (Reiskirchen-Lindenstruth, Germany). The resistance variation of the transducers has been measured with a Source Measurement Unit (SMU) 2450 from Tektronix® (Beaverton, Oregon, USA). The impedance of the transducers has been characterized from 500 Hz to 1 MHz with the impedance analyzer Keysight® E4990A (Santa Rosa, California, USA) and the impedance probe Keysight 42941A from the same vendor. Temperature characterization was conducted over a range from -30°C to 70°C, with intervals of 10°C, and each step lasting 15 min. The RH response testing was conducted at a constant temperature of 50°C, with RH levels set at 40%, 60%, and 80%, each step lasting 1h. The measured resistance is expressed as:

$$\Delta R/R_0 = \frac{R_T - R_0}{R_0} \quad (1)$$

where R_T is resistance in different testing temperatures, and R_0 is resistance at the lower temperature. The temperature coefficient of resistance (TCR) is mathematically calculated using the following expression:

$$TCR = \frac{\Delta R/R_0}{T_f - T_i} \times 100\% \quad (2)$$

where T_i and T_f represent the initial and the final temperature, respectively. The data was recorded during the last 4 min to ensure proper environmental steady-state. Additional measurement information, including the sensitivity of the sensor at each calibration point and the uncertainty of the measurements for temperature and humidity was calculated based on the method described in [36] and the values are reported in tables S.1-4.

3. Results and discussion

3.1 Material analysis condition

3.1.1 Raman spectroscopy

Raman spectra were acquired to examine the crystallography quality of the material resulting from laser irradiation. Figure 3a depicts normalized Raman spectra relative to the G peak of the induced material on PEI. In this spectra, two main peaks related to carbon-based materials are identified: D, G respectively at 1350 and 1580 cm^{-1} [37]. D peak is attributed to the defect of the structures generally due to the presence of covalently bonded oxygen. The G peak corresponds with the sp^2 hybridized carbon network of graphitic material. The crystallographic quality and electrical properties of the material are directly related to the I_G/I_D ratio and the full width at half maximum of the G peak ($FWHM_G$) [38]. In this case, the PEI sample exhibits a moderate I_G/I_D ratio, indicating relatively low structural disorder in the sp^2 graphitic lattice. Additionally, the $FWHM_G$ provides information on the defect level and uniformity of sp^2 clusters. Therefore, the moderate I_G/I_D ratio and high $FWHM_G$ explain the low conductivity of the LIG formed. The absence of the 2D peak at 2700 cm^{-1} further suggests that the spectrum is characteristic of glassy carbon [39].

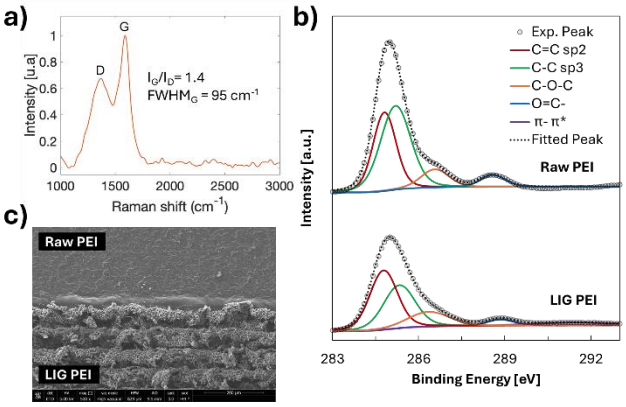

Figure 3. a) Normalized Raman spectrum of LIG on PEI. b) Deconvoluted C_{1s} peak before and after the laser. c) SEM images of LIG on PEI.

3.1.2 XPS spectra

XPS analysis was conducted to further examine the composition of the samples. Figure S.2 displays the general spectra of PEI substrate before and after laser treatment. After the laser irradiation, there is a noticeable decrease in the atomic concentration of O and N, as outlined in table S.5. This reduction can be attributed to the photothermal effect induced by the laser, which increases the temperature within the polymer lattice, causing weaker bonds (such as C-O and C-N) to break and release as gases (CO_2, O_2, N_2) [40]. Subsequently, the lattice recombines to form a graphitic-derived structure, as evidenced by the Raman spectra. The substrate exhibits a more reduced structure, with the C/O ratio increasing by over 3 times after laser treatment. This transformation is further

confirmed by the analysis of the deconvoluted C_{1s} peaks presented in figure 3b. For this material, four components were identified along with a π–π* satellite peak. Peaks at 284.8 eV and 285.3 eV were assigned to C=C sp^2 and C-C sp^3 hybridization states of carbon, respectively [41,42], while peaks at 286.3 eV and 288.7 eV were assigned to C-O-C and O=C- oxidized states of carbon, respectively [43,44]. As seen in figure 3b, there is a general decrease in the oxidized states after the laser treatment. This underscores the graphitization process, which involves the transformation of the sp^3 hybridization state, characteristic of the diamond crystal structure, into the sp^2 hybridization state typical of graphene and/or graphite [42]. The ratio $sp^2/(sp^2+sp^3)$ represents the degree of graphitization of the material. For our polymer, this ratio increased from 47% to 61% after laser irradiation. In conclusion, LIG on PEI demonstrated characteristics similar to amorphous or glassy carbon [29].

3.2 Thermistor characterization

3.2.1 Temperature result

The temperature response curves of the LIG thermistors for both designs are presented in figure 4. Both sensors exhibit a negative temperature coefficient (NTC), where resistance decreases with increasing temperature, as is typical for graphene and related materials [31–34]. Notably, over 7 cycles, both PEI transducers demonstrate high average TCR values (eq. 2) of -0.159 ± 0.019%/°C for the small design and -0.139 ± 0.011%/°C for the large design. This sensitivity can be attributed to the morphology of the LIG. As observed in the SEM image (Figure 3c), the LIG on PEI exhibits a porous and sectioned surface, composed of small interconnected conductive trenches formed by the laser ablation process. This results in an irregular LIG surface that, coupled with the low crystallographic quality of LIG (as assessed previously), leads to a high nominal resistance. Consequently, the PEI thermistor operates as a fragmented, highly resistive network. Both transducers demonstrate excellent linearity with R^2 over 0.98% throughout the entire temperature range with minimal hysteresis. Specifically, the maximum hysteresis variation is 0.4% and 0.7% for the large and small designs, respectively, at -10 °C. This information is summarized in table S.6.

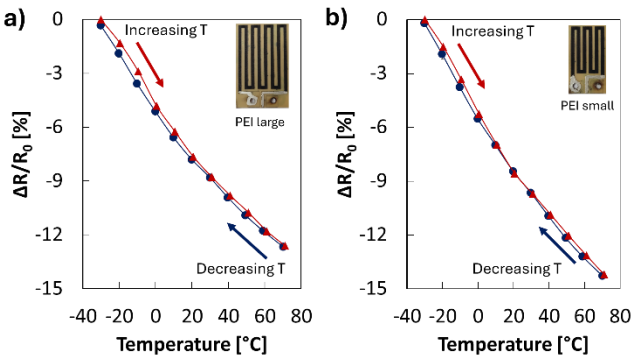

Figure 4. Resistance variation in the temperature range from -30 to 70 °C for a) PEI large design, b) PEI small design.

Figure 5 depicts the impact on the maximum, mean, and minimum resistance observed at -30 °C, 20 °C, and 70 °C, over 15 cycles of increasing and decreasing temperature. As shown, the deviation over time is minimal, with the resistance change starting to stabilize after approximately nine cycles. The difference in response between both designs can be attributed to the smaller surface area of the small design, where minor changes due to thermal expansion and thermal and mechanical stress have a greater impact on the overall resistance of the transducer, resulting in more significant deviations. The temporal variation of the large design traducer is shown in figure S.3, presenting a stable response during all cycles. Table 1 presents a comparison of this sensor with other recent work of carbon-based thermistors. In comparison, our transducer exhibits moderate sensitivities, excellent linearity, and slow response times in a very large temperature range which has not been tested yet. Moreover, due to its simple single fabrication step, the PEI thermistor emerges as a viable option for temperature sensing. From [33], the authors have extended the experimental results of a thermistor made on laser-reduced graphene oxide (LrGO) as depicted in figure S.5 and figure S.6, showcasing the resistive response across an extended temperature range. This sensor exhibits lower R^2 with a higher TCR, however, it requires additional fabrication steps involving chemicals, and the use of GO is well known to be highly sensitive to humidity, so it requires to be passivated to reduce the effect of humidity in the response [45].

Table 1. Comparison of recent resistive carbon-based temperature sensors.

Materials	Fabrication	Range (°C)	TCR (%/°C)	R^2	Rising/Falling time (s)	Reference
Graphene	CVD	30-70	-0.170	-	-	[46]
Graphene	Ink/laser	30-100	-0.177	>0.86	-	[47]
rGO	LrGO	-30-35	-0.488	-	-	[33]

rGO	LrGO	-30-70	-0.671	0.95	-	Extended from [33]
rGO/PDMS	LrGO	20-50	-0.380	0.99	-	[45]
PI/rGO	LIG	25-45	-1.56	-	13.5/26.2	[34]
PI/PDMS	LIG	20-100	0.250	0.98	2.6/7.9	[30]
Paper	LIG	10-60	-0.280	0.99	-	[20]
PI	LIG	20-60	-0.111	-	-	[31]
PI	LIG	30-40	-0.041	-	-	[32]
PEI	LIG	-30-70	-0.159	0.98	78.0/65.0	This work

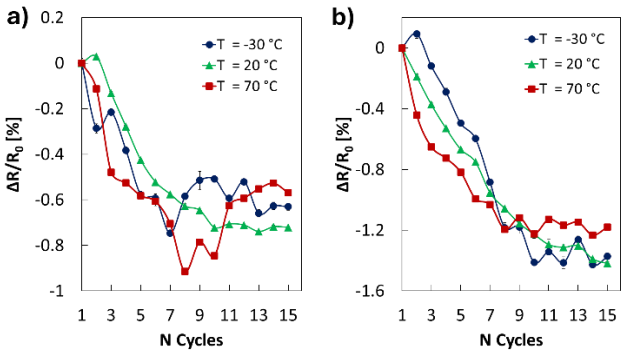

Figure 5. Resistance variation over cycles at -30 °C, 20 °C and 70 °C for a) PEI large design, b) PEI small design.

Additionally, the time response of the sensors is presented in figure 6. As depicted, our transducer presents long response times to temperature changes from 20 to 40 °C at 35% RH, with falling times and rising times of 66.7 s and 63.1 s for the large design, and 65.0 s and 78.0 s for the small design.

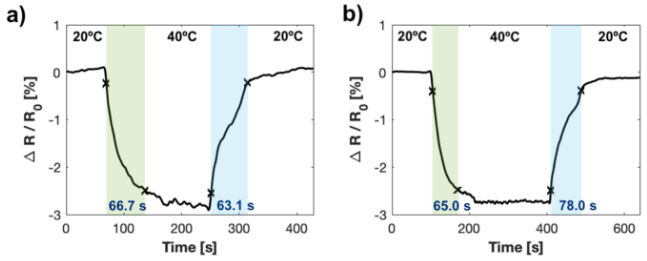

Figure 6. Falling and rising time at 20 °C to 40 °C at 35%RH for a) PEI large design, b) PEI small design.

3.2.2 Humidity effect

Figure 7 presents the effect of the RH (from 40% to 80% at 50 °C) on the transducer. As observed, our sensor exhibits a negative humidity coefficient. The measured sensitivities are -0.017 ± 0.005%/RH% and -0.015 ± 0.007%/RH% for two sensors over 3 cycles for the large and small designs, respectively. These values are relatively low compared to the thermal sensitivity of the devices. Both designs exhibited moderate hysteresis and linearity, with specific values provided in table S.7.

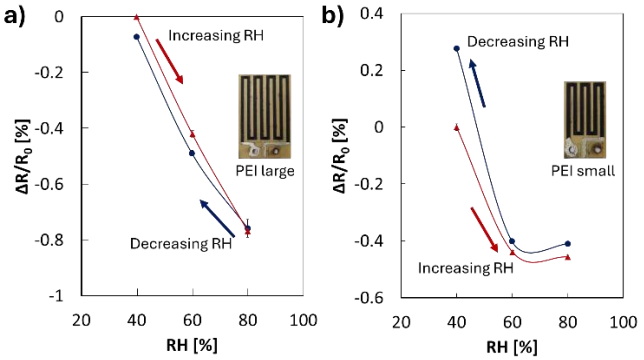

Figure 7. Resistance variation in the RH ranges from 40 to 80% RH at 50 °C for a) PEI large design, b) PEI small design.

This is an advantage over other LIG precursors, such as PI, which is widely used as a sensing layer for humidity sensors due to its great capacity to absorb moisture and modify electrical characteristics [48,49]. In contrast, the higher resistance of LIG on PEI means that humidity induces a slight decrease in resistance due to improved ionic conduction through adsorbed water compared to the overall resistance [50]. Based on these findings, PEI-based transducers are preferable for temperature sensing due to their higher sensitivity, low humidity impact, and minimal hysteresis compared to other LIG sensors. Additionally, it is possible to

eliminate the effects of humidity on the sensor by using a coating such as polydimethylsiloxane (PDMS) [51].

3.2.3 Bending effect

The flexibility of the sensors was assessed by subjecting them to 300 cycles of bending at a curvature of 35 m^{-1} under ambient conditions. The evolution of the resistance over the cycles for both transducers is depicted in Figure S.7. The result indicates a 7.8% and 22.5% increase in resistance after all the cycles for the large and small designs, respectively. The increment in resistance from normal to elongated position is 1.4% and 8.0% for the large and small designs, respectively. This increase in resistance is attributed to the elongation of the sensor, which increases the separation between LIG conductive zones during elongation, resulting in an increased resistance [52]. In the smaller design, this effect has a more significant impact on the overall resistance relative to the total length of the sensor. Compared to the larger design, the smaller sensor exhibits a greater deformation of the pattern, resulting in a more substantial increase in resistance. These results show that although the sensors are bendable, their response is significantly affected by the bending effect. As a result, proper calibration is necessary to compensate for this issue. Therefore, the sensor is well-suited for free-form surfaces but may not be ideal for applications involving both bending and temperature stimuli.

4. Conclusions

In this study, two resistive temperature sensors were fabricated on polyetherimide (PEI) using different design sizes. The substrate was subjected to laser scribing to produce laser-induced graphene. The induced material was characterized through Raman, XPS spectroscopy and SEM, confirming the successful formation of graphitic-based LIG.

In terms of temperature response, both sensors exhibited good sensitivity, excellent linearity (R^2 >0.98), and low hysteresis, demonstrating good temperature sensitivity with -0.159%/°C. The impact of humidity was also evaluated, showing good independence from humidity, which can be further enhanced by using protective coatings. Additionally, the bending effect was investigated, revealing low variation over cycles for both designs. The results indicate that the size of the design has a low impact on the behaviour, with the smaller design performing slightly better overall.

In summary, the findings of this study highlight PEI as an excellent substrate for LIG thermistors, offering flexible and cost-effective material with low humidity dependence, excellent linearity, and good sensitivity. The insights gained into material selection and sensor design provide valuable knowledge, facilitating a transition towards more sustainable and environmentally friendly practices in flexible electronics production.

Conflict of interest

The authors declare no conflict of interest.

Data Availability Statement

The data that support the findings of this study are available from the corresponding author upon reasonable request.

Acknowledgements

This work was partially funded by the Spanish Ministry of Sciences and Innovation through the National Projects: PID2020-117344RB-I00, CNS2022-135915, PRE2021-096886, TED2021-129949A-I00 funded by MCIN/AEI/ 10.13039/501100011033; and the Ramón y Cajal fellow RYC2019-027457-I. This work has also been funded by the Junta de Andalucía – Consejería de Universidad, Investigación e Innovación through the projects ProyExcel_00268 and P21_00105 through FEDER funds. SEM, Raman and XPS spectroscopy were conducted at the Scientific Instrumentation Center (CIC) of the University of Granada.

References

[1] Maskey B B, Shrestha K, Sun J, Park H, Park J, Parajuli S, Shrestha S, Jung Y, Ramasundaram S, Koirala G R, and others 2020 Proving the robustness of a PEDOT: PSS-based thermistor via functionalized graphene oxide–poly (vinylidene fluoride) composite encapsulation for food logistics *Rsc Advances* **10** 12407–14

[2] Chen R, Luo T, Geng D, Shen Z and Zhou W 2022 Facile fabrication of a fast-response flexible temperature sensor via laser reduced graphene oxide for contactless human-machine interface *Carbon* **187** 35–46

[3] Su Y, Ma C, Chen J, Wu H, Luo W, Peng Y, Luo Z, Li L, Tan Y, Omisore O M, and others 2020 Printable, highly sensitive flexible temperature sensors for human body temperature monitoring: a review *Nanoscale Research Letters* **15** 1–34

[4] Lau A H Y, Chik G K K, Zhang Z, Leung T K W and Chan P K L 2020 Conformal devices for thermal sensing and heating in biomedical and human–machine interaction applications *Advanced Intelligent Systems* **2** 2000005

[5] Wang Y-F, Sekine T, Takeda Y, Yokosawa K, Matsui H, Kumaki D, Shiba T, Nishikawa T and Tokito S 2020 Fully printed PEDOT: PSS-based temperature sensor with high humidity stability for wireless healthcare monitoring *Scientific reports* **10** 2467

[6] Nenov T and Yordanov S P 2020 *Ceramic sensors: technology and applications* (CRC press)

[7] Kim B-J, Lee Y W, Chae B-G, Yun S J, Oh S-Y, Kim H-T and Lim Y-S 2007 Temperature dependence of the first-order metal-insulator transition in VO2 and programmable critical temperature sensor *Applied Physics Letters* **90** 023515

[8] Chen J, Zhu Y, Guo Z and Nasibulin A G 2020 Recent progress on thermo-electrical properties of conductive polymer composites and their application in temperature sensors *Engineered Science* **12** 13–22

[9] Davaji B, Cho H D, Malakoutian M, Lee J-K, Panin G, Kang T W and Lee C H 2017 A patterned single layer graphene resistance temperature sensor *Scientific reports* **7** 1–10

[10] Nag A, Simorangkir R B V B, Gawade D R, Nuthalapati S, Buckley J L, O'Flynn B, Altinsoy M E and Mukhopadhyay S C 2022 Graphene-based wearable temperature sensors: A review *Materials & Design* **221** 110971

[11] Soni M, Bhattacharjee M, Ntagios M and Dahiya R 2020 Printed temperature sensor based on PEDOT: PSS-graphene oxide composite *IEEE Sensors Journal* **20** 7525–31

[12] Seifi M, Hamedi S and Kordrostami Z 2022 Fabrication of a high-sensitive wearable temperature sensor with an improved response time based on PEDOT: PSS/rGO on a flexible kapton substrate *Journal of Materials Science: Materials in Electronics* **33** 6954–68

[13] Monea B F, Ionete E I, Spiridon S I, Ion-Ebrasu D and Petre E 2019 Carbon nanotubes and carbon nanotube structures used for temperature measurement *Sensors* **19** 2464

[14] Beloin-Saint-Pierre D and Hischier R 2021 Towards a more environmentally sustainable production of graphene-based materials: Building on current knowledge to offer recommendations *The International Journal of Life Cycle Assessment* **26** 327–43

[15] Ghulam A N, Dos Santos O A, Hazeem L, Pizzorno Backx B, Bououdina M and Bellucci S 2022 Graphene oxide (GO) materials—Applications and toxicity on living organisms and environment *Journal of Functional Biomaterials* **13** 77

[16] Lin J, Peng Z, Liu Y, Ruiz-Zepeda F, Ye R, Samuel E L, Yacaman M J, Yakobson B I and Tour J M 2014 Laser-induced porous graphene films from commercial polymers *Nature communications* **5** 5714

[17] Wang L, Wang Z, Bakhtiyari A N and Zheng H 2020 A comparative study of laser-induced graphene by CO2 infrared laser and 355 nm ultraviolet (UV) laser *Micromachines* **11** 1094

[18] Chyan Y, Ye R, Li Y, Singh S P, Arnusch C J and Tour J M 2018 Laser-induced graphene by multiple lasing: toward electronics on cloth, paper, and food *ACS nano* **12** 2176–83

[19] C. Claro P I, Pinheiro T, Silvestre S L, Marques A C, Coelho J, Marconcini J M, Fortunato E, C. Mattoso L H and Martins R 2022 Sustainable carbon sources for green laser-induced graphene: A perspective on fundamental principles, applications, and challenges *Applied Physics Reviews* **9** 041305

[20] Kulyk B, Silva B F, Carvalho A F, Barbosa P, Girão A V, Deuermeier J, Fernandes A J, Figueiredo F M, Fortunato E and Costa F M 2022 Laser-induced graphene from paper by ultraviolet irradiation: humidity and temperature sensors *Advanced Materials Technologies* **7** 2101311

[21] Houeix Y, Gerardo D, Gómez-Gijón S, Toral V, Rodríguez N, Morales D P and Rivadeneyra A 2024 Responsible Humidity Sensor by Direct Laser Writing on Cork Substrate *Advanced Sustainable Systems* **n/a** 2300606

[22] Zhu J, Huang X and Song W 2021 Physical and chemical sensors on the basis of laser-induced graphene: mechanisms, applications, and perspectives *ACS nano* **15** 18708–41

[23] Le T-S D, Phan H-P, Kwon S, Park S, Jung Y, Min J, Chun B J, Yoon H, Ko S H, Kim S-W, and others 2022 Recent advances in laser-induced graphene: mechanism, fabrication, properties, and applications in flexible electronics *Advanced Functional Materials* **32** 2205158

[24] Tavakkoli Gilavan M, Rahman M S, Minhas-Khan A, Nambi S and Grau G 2021 One-Step Fabrication of Low-Resistance Conductors on 3D-Printed Structures by Laser-Induced Graphene *ACS Applied Electronic Materials* **3** 3867–75

[25] Yazdi A Z, Navas I O, Abouelmagd A and Sundararaj U 2017 Direct Creation of Highly Conductive Laser-Induced Graphene Nanocomposites from Polymer Blends *Macromolecular Rapid Communications* **38** 1700176

[26] de Lima L F and de Araujo W R 2022 Laser-scribed graphene on polyetherimide substrate: an electrochemical sensor platform for forensic determination of xylazine in urine and beverage samples *Microchimica Acta* **189** 465

[27] Yang W, Zhao W, Li Q, Li H, Wang Y, Li Y and Wang G 2019 Fabrication of smart components by 3D printing and laser-scribing technologies *ACS applied materials & interfaces* **12** 3928–35

[28] Wang G, Tao L-Q, Peng Z, Zhu C, Sun H, Zou S, Li T, Wang P, Chen X and Ren T-L 2022 Nomex paper-based double-sided laser-induced graphene for multifunctional human-machine interfaces *Carbon* **193** 68–76

[29] Houeix Y, Romero F J, Moraila C L, Rivadeneyra A, Rodriguez N, Morales D P and Salinas-Castillo A 2023 Laser-synthesis of conductive carbon-based materials from two flexible commercial substrates: A comparison *Applied Surface Science* **634** 157629

[30] Guo J, Liu X, Sun Z, Zheng X, Sung H-K, Yao Z, Li Y and Li Y 2024 An intelligent dual-sensing e-skin system for pressure and temperature detection using laser-induced graphene and polydimethylsiloxane *Materials & Design* **238** 112640

[31] Marengo M, Marinaro G and Kosel J 2017 Flexible temperature and flow sensor from laser-induced graphene *2017 IEEE SENSORS* (IEEE) pp 1–3

[32] Kun H, Bin L, Orban M, Donghai Q and Hongbo Y 2021 Accurate flexible temperature sensor based on laser-induced graphene material *Shock and Vibration* **2021** 1–7

[33] Romero F J, Rivadeneyra A, Toral V, Castillo E, García-Ruiz F, Morales D P and Rodriguez N 2018 Design guidelines of laser reduced graphene oxide conformal thermistor for IoT applications *Sensors and Actuators A: Physical* **274** 148–54

[34] Han R, Wang L, Tang X, Qian J, Yu J, Chen X and Huang Y 2021 Facile fabrication of rGO/LIG-based temperature sensor with high sensitivity *Materials Letters* **304** 130637

[35] Anon 1997 Standard Test Method for Sheet Resistance Uniformity Evaluation by In-Line Four- Point Probe with the Dual-Configuration Procedure *American society for testing and materials* **10.04** 13

[36] White D R, Hill K, del Campo D and Garcia Izquierdo C 2014 Guide on secondary thermometry: Thermistor thermometry *Bureau International des Poids et Mesures: Paris, France*

[37] Wu J-B, Lin M-L, Cong X, Liu H-N and Tan P-H 2018 Raman spectroscopy of graphene-based materials and its applications in related devices *Chemical Society Reviews* **47** 1822–73

[38] Mohan V B, Nieuwoudt M, Jayaraman K and Bhattacharyya D 2017 Quantification and analysis of Raman spectra of graphene materials *Graphene Technology* **2** 47–62

[39] Muzyka K and Xu G 2022 Laser-induced Graphene in Facts, Numbers, and Notes in View of Electroanalytical Applications: A Review *Electroanalysis* **34** 574–89

[40] Zhang Z, Zhu H, Zhang W, Zhang Z, Lu J, Xu K, Liu Y and Saetang V 2023 A review of laser-induced graphene: From experimental and theoretical fabrication processes to emerging applications *Carbon* **214** 118356

[41] Xie F, Xie W, Gong L, Zhang W, Chen S, Zhang Q and Chen J 2010 Surface characterization on graphitization of nanodiamond powder annealed in nitrogen ambient *Surface and Interface Analysis* **42** 1514–8

[42] Aboua K A M, Umehara N, Kousaka H, Tokoroyama T, Murashima M, Mustafa M M B, Mabuchi Y, Higuchi T and Kawaguchi M 2020 Effect of mating material and graphitization on wear of aC: H coating in boundary base oil lubrication *Tribology Letters* **68** 1–8

[43] Burrell M C and Chera J J 1999 Polyetherimide (Ultem®) spin cast films by XPS *Surface Science Spectra* **6** 18–22

[44] Louette P, Bodino F and Pireaux J-J 2005 Polyimide XPS reference core level and energy loss spectra *Surface Science Spectra* **12** 121–6

[45] Romero F J, Rivadeneyra A, Becherer M, Morales D P and Rodríguez N 2020 Fabrication and characterization of humidity sensors based on graphene oxide–PEDOT: PSS composites on a flexible substrate *Micromachines* **11** 148

[46] Rajan G, Morgan J J, Murphy C, Torres Alonso E, Wade J, Ott A K, Russo S, Alves H, Craciun M F and Neves A I 2020 Low operating voltage carbon–graphene hybrid E-textile for temperature sensing *ACS applied materials & interfaces* **12** 29861–7

[47] Kumar S, Bhatt K, Kumar P, Sharma S, Kumar A and Tripathi C 2019 Laser patterned, high-power graphene paper resistor with dual temperature coefficient of resistance *RSC advances* **9** 8262–70

[48] Wang N, Tong J, Wang J, Wang Q, Chen S and Sheng B 2022 Polyimide-sputtered and polymerized films with ultrahigh moisture sensitivity for respiratory monitoring and contactless sensing *ACS Applied Materials & Interfaces* **14** 11842–53

[49] Rivadeneyra A, Fernández-Salmerón J, Agudo M, López-Villanueva J A, Capitan-Vallvey L F and Palma A J 2014 Design and characterization of a low thermal drift capacitive humidity sensor by inkjet-printing *Sensors and Actuators B: Chemical* **195** 123–31

[50] Chen M-C, Hsu C-L and Hsueh T-J 2014 Fabrication of humidity sensor based on bilayer graphene *IEEE Electron Device Letters* **35** 590–2

[51] V. Toral, Y. Houeix, D. Gerardo, I. Blasco-Pascual, A. Rivadeneyra, and F. J. Romero 2024 Graphene-Enabled Wearable for Remote ECG and Body Temperature Monitoring *IEEE Journal on Flexible Electronics* **3** 159–68

[52] Carvalho A F, Fernandes A J, Martins R, Fortunato E and Costa F M 2020 Laser-induced graphene piezoresistive sensors synthesized directly on cork insoles for gait analysis *Advanced Materials Technologies* **5** 2000630